Published in final edited form as:
J Chem Inf Model. 2011 December 27; 51(12): 3262–3274. doi:10.1021/ci200435b.

Structure-based prediction of subtype-selectivity of Histamine H_3 receptor selective antagonists in clinical trials

Soo-Kyung Kim[1], **Peter Fristrup**[2], **Ravinder Abrol**[1], and **William A. Goddard III**[1,*]

[1]Materials and Process Simulation Center (MC139-74), California Institute of Technology, 1200 E. California Blvd., Pasadena, CA 91125

[2]Department of Chemistry, Technical University of Denmark, Kemitorvet, Building 201, 2800 Lyngby, Denmark

Abstract

Histamine receptors (HRs) are excellent drug targets for the treatment of diseases such as schizophrenia, psychosis, depression, migraine, allergies, asthma ulcers, and hypertension. Among them, the human H_3 Histamine receptor (hH_3HR) antagonists have been proposed for specific therapeutic applications, including treatment of Alzheimer's disease, attention deficit hyperactivity disorder (ADHD), epilepsy, and obesity.[1] However, many of these drug candidates cause undesired side effects through the cross-reactivity with other histamine receptor subtypes. In order to develop improved selectivity and activity for such treatments it would be useful to have the three dimensional structures for all four HRs. We report here the predicted structures of four HR subtypes (H_1, H_2, H_3, and H_4) using the GEnSeMBLE (GPCR Ensemble of Structures in Membrane BiLayer Environment) Monte Carlo protocol.[2] sampling ~ 35 million combinations of helix packings to predict the 10 most stable packings for each of the four subtypes. Then we used these best 10 protein structures with the DarwinDock Monte Carlo protocol to sample ~ 50,000*20 poses to predict the optimum ligand-protein structures for various agonists and antagonists. We find that $E206^{5.46}$ contributes most in binding H_3 selective agonists (**5**, **6**, **7**) in agreement with experimental mutation studies. We also find that conserved E5.46/ S5.43 in both of hH_3HR and hH_4HR are involved in H_3/ H_4 subtype selectivity. In addition, we find that $M378^{6.55}$ in hH_3HR provides additional hydrophobic interactions different from hH_4HR (the corresponding amino acid of $T323^{6.55}$ in hH_4HR) to provide additional subtype bias. From these studies we developed a pharmacophore model based on our predictions for known hH_3HR selective antagonists in clinical study [ABT-239 **1**, GSK-189,254 **2**, PF-3654746 **3**, and BF2.649 (Tiprolisant) **4]** that suggests critical selectivity directing elements are: the basic proton interacting with $D114^{3.32}$, the spacer, the aromatic ring substituted with the hydrophilic or lipophilic groups interacting with lipophilic pockets in TMs 3-5-6 and the aliphatic ring located in TMs 2-3-7. These 3D structures for all four HRs should help guide the rational design of novel drugs for the subtype selective antagonists and agonists with reduced side effects.

[*]**CORRESPONDING AUTHOR FOOTNOTE**. phone: 1-626-395-2731; FAX: 1-626-585-0918; wag@wag.caltech.edu.
AUTHOR EMAIL ADDRESS: Soo-Kyung Kim: skkim@wag.caltech.edu; Peter Fristrup: pf@kemi.dtu.dk; Ravinder Abrol: abrol@wag.caltech.edu: William A. Goddard III: wag@wag.caltech.edu

Supporting Information Available: The sequence identities of four human Histamine receptors (HRs) and the x-ray structures, turkey β_1 adrenergic receptor, human β_2 adrenergic receptor ($h\beta_2AR$), human adenosine A_{2A} receptor ($hAA_{2A}R$), and bovine rhodopsin (Table S1), Overview over residue numbering for the transmembrane (TM) regions in each of the four histamine receptors (HR) based on homology to turkey β_1 adrenergic receptor ($t\beta_1AR$) and human β_2 adrenergic receptor (Table S2). This information is available free of charge via the Internet at http://pubs.acs.org.

Keywords

Membrane protein structure; binding; docking; modeling; receptor; ligand

INTRODUCTION

Histamine receptors (HRs) are aminergic G protein-coupled receptors (GPCRs) with 7 transmembrane (TM)-spanning helices serving as a mediator in hypersensitivity (allergic) responses, gastric acid secretion, neurotransmission, immunemodulation, cell differentiation, and embryonic development, among others.[3] Four subtypes of human HRs, H_1, H_2, H_3, and H_4, have been identified.[4] All HRs are excellent drug targets for the treatment of such diseases as schizophrenia, Alzheimer's disease (AD), dementia, anxiety, tremor (Parkinson's disease), attention deficit hyperactivity disorder (ADHD), mood disorders, sleep disorders (narcolepsy), depression, migraine, allergies, asthma ulcers, stroke, epilepsy, obesity, diabetes, and cancer.[5] Indeed human histamine H_1 receptor (hH_1HR) antagonists (antihistamine) are widely used in the treatment of allergy.[6] In addition, hH_2HR antagonists are used in treating peptic ulcers, gastroesophageal reflux disease, and gastrointestinal bleeding.[7, 8] The hH_3HR antagonists have been proposed for such therapeutic applications as treatment of Alzheimer's disease, attention deficit hyperactivity disorder (ADHD), epilepsy, and obesity.[1] The hH_4HR has been suggested as an interesting drug target for the therapy of inflammation, allergy, and autoimmune disorders.[9]

While hH_1HR, hH_2HR, and hH_4HRs have been successful targets of blockbuster drugs for treating allergic diseases, gastric ulcer, and chronic constipation, the development of hH_3HR ligands still lag on their way to market, at least partly because of problems with selectivity. Thus, we decided to focus on developing an understanding of how to make ligands selective for hH_3HR.

Section 1 in Results and Discussions describes the prediction of 3D structures for all four subtypes (H_1, H_2, H_3, and H_4) of hHRs, using the GEnSeMBLE (GPCR Ensemble of Structures in Membrane BiLayer Environment) method[2] for generating the ensemble of the 10 most stable 3D structures of these GPCRs.

Then section 2 in Results and Discussions reports the predictions from the DarwinDock method of the binding sites for structurally known antagonists **1**, **2**, **3**, **4** now in clinical studies, three agonists (**5**, **6**, **7**), five antagonists (clobenpropit **8** *N*'-[(4-chlorophenyl)methyl]-1-[3-(3H-imidazol-4-yl)propylsulfanyl]formamidine, ciproxifan **9**, thioperamide **10**, A-304121 [4-(3-((2R)-2-aminopropanoyl-1-piperazinyl)propoxy)phenyl)cyclopropylmethanone] **11**, A-317920 [N-((1R)-2-(4-(3-(4-(cyclopropylcarbonyl)phenoxy)propyl)-1-piperazinyl)-1-methyl-2-oxo-ethyl-)-2-furamide] **12** for the structure-activity relationship (SAR) studies.[10]

The section 3 extends the comparison of the 3D structure of our predicted structure with the recently reported 3.1 Å crystal structure of the hH_1HR–T4-lysozyme fusion protein (H1R–T4L) complex with doxepin.[11] Since we predicted the 3D structure of all HRs when no x-ray structure of the HRs was available, this comparison will validate our methods. The 1.3 Å root mean squared deviation (RMSD) in TM between two structures reveals our atomic details of binding site and model will be highly useful for guiding rational design of ligands with high H_3HR selectivity.

RESULTS AND DISCUSSIONS

1. GEnSeMBLE predictions of apo-protein structures for all four HRs

The seven TM domains of 4 hHRs in Fig. 1 were predicted by PredicTM which combines hydrophobicity analysis and multiple sequence alignment of sequences using the MAFFT[12] program. Hydrophobic profile in the multiple sequence alignment (using the thermodynamic and biological hydrophobic scales from White and von Heijne[13, 14] shows all hHRs have 7-TM characters as shown in GPCRs. hH_2HR has a shorter intracellular 3 loop compared to other subtypes. Fig. 2 shows the final TM regions and multiple alignments of all HRs from PredicTM. All TM regions of four subtypes applied by capping rules are in good agreement within 1 to 5 residue difference at the terminal end.

The GEnSeMBLE method[2] was used to predict the 3D structure of all four HRs before the x-ray structure of the H_1HR was reported.[11] In GEnSeMBLE we start with some template structure and consider 12 rotations (30° pitch) about the helix axis for each of the 7 TM regions, leading to $(7)^{12}$ ~35 million packings. We then estimate the energy for all 35 million based on the pairwise interactions of the 12 strongly interacting pairs. In these calculations we start with several experimental and computational templates and finally select those with the best total interaction energies.

However when we started this project x-ray crystal structures were avaible for the human β_2 adrenergic receptor (PDB: 2RH1)[15] and the turkey β_1 adrenergic receptor (PDB: 2VT4),[16] Consequently we deviated from our standard methodology for predicting histamine receptor structures as follows:

First, the TM regions in the two templates were identified and the corresponding regions in the four histamine receptors identified based on the higher sequence homology in the TM regions (Table S1). Overviews over which residues are part of the TM region for each of the four HRs are shown in Table S2.

Then, each TM was mutated to match the HR of interest and energy-minimized *in vacuous*. Then the 7 helix bundle was used as input to the BiHelix protocol of GEnSeMBLE[2] in which 144 combinations are considered for each pair each with re-optimized side chains. Here, each of the seven TM was rotated systematically ±90° using a 15° sampling interval, leading to structures for the packed bundle. Then we superimposed the BiHelix energies to estimate the 1000 energetically most favored 7 TM helix bundles. These bundles were then built, the side-chains re-optimized [using the SCREAM procedure[17]] and the total energies were calculated using both the standard charged model (where Asp, Glu, Lys, Arg have net charges) and neutral model we have developed.[18] From these 1000 we collected the best 10 into Table 1 for each combination of HR and template. These results make it clear that for hH_1HR and hH_3HR the structures derived from the human β_2 adrenergic receptor were significantly more favorable energetically than models derived from the turkey β_1 adrenergic receptor. In contrast, for hH_2HR and hH_4HR the structures derived from the turkey β_1 adrenergic receptor were most favorable.

For these best 10 structures we examine new confituraitons including rotations of ±15° for TM3, −15, ±30, 45° for TM4, 15° for TM5. We found that the structure derived directly from the initial helix bundle (i.e. with $\eta = 0°$ for all 7 helices) was not unreasonably high in energy. This preference for structures near 0° supports the applicability of these two x-ray crystal structures as a reasonable starting point for the BiHelix sampling. Indeed, the top-scoring structures for all four HRs differed in the rotation of only a single *one* of the seven TMs. For hH_3HR the top-scoring model had a −30° rotation of TM4 (human β_2 adrenergic receptor as template), whereas for hH_1HR the top-scoring model had a +15° rotation of TM4

(human β_2 adrenergic receptor as template). Moreover for hH_2HR the top-scoring model had a −15° rotation of TM4 (turkey β_1 adrenergic receptor as template) while for hH_4HR the top-scoring model had a +15° rotation of TM5 (turkey β_1 adrenergic receptor as template).

hH_4HR has a sequence identity of 34.83% to hH_3HR and 54.84% in TM region compared with hH_1HR (20.90% in overall, 32.15% in TM) and hH_2HR (17.30% in overall, 33.08 in TM) with low sequence identity in Table S1 in Supporting information. Many compounds with reported affinity for hH_3HR also have affinity for hH_4HR. Compounds like clozapine, clobenpropit behave as partial agonists at hH_4HR and as antagonists at hH_3HR showing some functional selectivity.[19] Many drug candidates cause undesired side effects through their cross-reactivity. To develop improved selectivity and activity for such treatments we use the 10 most stable three dimensional structures for all four HRs.

2. Predicted structures for ligands binding to all four HRs

First generation hH_3HR antagonists were monoalkyl-substituted imidazole-based derivatives like thioperamide, clobenpropit or ciproxifan.[20] Potent stimulation of hH_3HR has been observed by imidazole derivatives only. Claimed interaction potential to CYP isozymes caused by the imidazole moiety related to elements of the porphyrine cycle and sometimes complex pharmacological behavior led to imidazole replacements. A general pharmacophore element of these non-imidazole derivatives has been described which is nowadays shown in numerous variations and combinations: A basic moiety is linked by a spacer to a central, mostly aromatic core structure which then is connected to further affinity enhancing elements, e.g. another basic moiety or hydrophilic/ lipophilic groups or a combination thereof.[21]

A number of hH_3HR antagonists have advanced to the clinical area for the potential treatment of human cognitive disorders.[22] These include 4-(2-{2-[(2R)-2-Methylpyrrolidin-1-yl]ethyl}-benzofuran-5-yl)benzonitrile, (ABT-239 **1**), 6-[(3-cyclobutyl-2,3,4,5-tetrahydro-1H-3-benzazepin-7-yl)oxy]-Nmethyl-3-pyridinecarboxamide hydrochloride (GSK189254 **2**), (1R,3R)-N-ethyl-3-fluoro-3-[3-fluoro-4-(pyrrolidin-1-ylmethyl)phenyl]cyclobutane-1-carboxamide (PF-03654746 **3**), 1-{3-[3-(4-chlorophenyl)propoxy]propyl} piperidine hydrochloride (BF2.649 **4**), MK-0249 (structure not yet disclosed), JNJ-17216498 (structure not yet disclosed), and ABT-288 (structure not yet disclosed).

Among these, we selected structurally known compounds (structures shown in Chart 1) like ABT-239 **1** (pKi: 9.35 at hH_3HR), for cognitive disorder (Phase I),[23] GSK-189254A **2** (pKi: 9.59 at hH_3HR) for dementia, narcolepsy, schizophrenia (Phase I),[24] PF-3654746 **3** (pKi: 8.49 at hH_3HR) for allergic rhinitis (Phase II), and BF2.649 **4** (tiprolisant, pKi: 8.3 at hH_3HR) for central nervous system disease: hypersommina, narcolepsy (Phase II)[25] for docking studies.

As summarized in Methods the DarwinDock method for predicting ligand binding sites, starts by sampling the full protein to locate putative binding regions, and then aims at sampling a complete set of ligand conformation (~20) for each of which we sample a complete set of poses (~50,000), from which we select the best poses using the total binding energy, E.

2.1 Endogenous agonist histamine—We docked histamine, the endogenous agonist **5**, to the lowest E predicted structure of hH_3HR in Table 1 from CombiHelix.

Most of poses show salt-bridges at $D114^{3.32}$ or $E206^{5.46}$ with the protonated nitrogen atom or the one of the nitrogen atoms in the imidazole ring. Our cavity analysis (Table 2) of the

histamine bound to hH_3HR shows that the major contributing amino acids in ligand binding are $E206^{5.46}$ (−5.08 kcal/mol), $F207^{5.47}$ (−3.81 kcal/mol), $Y115^{3.33}$ (−3.09 kcal/mol), and $D114^{3.32}$ (−2.12 kcal/mol) based on non-bonding energies [defined in the methods section as the sum of vdW, electrostatic Coulomb with 2.5 dielectric constant and H-bond energies]. This result agrees with previous docking studies which all shows hydrophilic interactions at $D114^{3.32}$/ $E206^{5.46}$ and hydrophobic interactions at $Y115^{3.33}$, $Y374^{6.51}$, and $F398^{7.39}$ as found in bovine rhodopsin based hH_3HR homology models.[26] Histamine has similar interactions in hH_4HR with the main interaction at $D114^{3.32}$/ $E206^{5.46}$.[27, 28] Supporting this, the Ala mutation of $E206^{5.46}$ which was the most major contributing residue in the cavity analysis (Table 2) shows dramatic loss of agonist with more than 2,000-fold decrease. In addition, $T204A^{5.44}$ and $A202Q^{5.42}$ mutants display substantial decrease of histamine binding with 5.7 and 4.2-fold decrease compared with the wild-type, respectively.[26]

In the neutral system of histamine-hH_3HR, we find that the de-protonated nitrogen atom of the histamine interacts with the protonated $D114^{3.32}$, while the protonated $E206^{5.46}$ also H-bonds with the ε-NH atom in the imidazole ring of histamine, as shown in Fig. 3. An additional hydrophobic interaction occurs at $F207^{5.47}$ and $Y115^{3.33}$.

2.2. hH_3HR selective agonists, 5, 6, 7—We next matched the H_3 selective agonist, (*R*)-α-methyl histamine **6**, to validate the binding site of histamine at hH_3HR, leading to common interactions at $E206^{5.46}$ (−4.73 kcal/mol), $F207^{5.47}$ (−3.99 kcal/mol), $D114^{3.32}$ (−2.96 kcal/mol), and $Y115^{3.33}$ (−2.38 kcal/mol). However, the stereoisomer, (*S*)-α-methyl histamine **7**, with ~100-fold less binding affinity reveals unfavorable interactions at $Y115^{3.33}$ (+6.84 kcal/mol) because of the bad contact with the α-methyl group (Table 3 and Fig. 4). The result is a dramatic decrease in binding affinity (cavity sum = −18.07 for (*R*)-α-methyl histamine **6** vs. −8.39 for (*S*)-α-methyl histamine **7**) in agreement with the dramatically decreased experimental binding affinity of (*S*)-α-methyl histamine **7** at hH_3HR (PKi at hH_3HR: 8.2 for **6** vs 7.2 for **7**).[29]

The cavity analysis of the H_3 selective agonists (**5**, **6**, **7**) suggests the major contributing amino acid is $E206^{5.46}$ (Table 2 and 3). These docking results are in good agreement with the current mutational study. The most pronounced reduction in potency and affinity of the agonists was seen with the mutation of $E206^{5.46}$.[26]

Thus the stereoselectivity of the methylated histamine derivatives are explained by these docking studies. The result agrees with experimental observations, that the methylated histamine derivative, (*R*)-α-methylhistamine is the more selective and the potent hH_3HR agonist. The (*S*)-stereo isomer is about 100 times less potent than the (*R*)-isomer.[29]

2.3 Docking of hH_3HR selective antagonist 8, clobenpropit, at all four HRs and further SAR studies—Antagonist docking started from the assumption that classical H_3 antagonists such as monoalkyl-substituted imidazole-based derivatives would share the interaction between their imidazole ring and $E206^{5.46}$ as shown in the endogenous agonist, histamine **5**. This hypothesis is based on the partial structural similarity between histamine and imidazole-containing H_3 antagonists (i.e., the imidazole ring, the spacer, and the basic or polar portion).

We docked hH_3HR selective antagonist **8**, clobenpropit, to the lowest E predicted structures of all four hHRs of Table 1. From the cavity analysis of H_3 subtype selective clobenpropit **8** bound to hH_3HR, Table 4 shows that the major contributing amino acids are $Y115^{3.33}$ (−4.96 kcal/mol), $W402^{7.43}$ (−4.71 kcal/mol), and $D114^{3.32}$ (−3.73 kcal/mol). The major H-bonding is shown at $D114^{3.32}$ and $Y374^{6.51}$ with the isothiourea group. Additional H-bonding with the terminal imidazole ring is formed at $E206^{5.46}$. The *para*-chloro-benzyl

group of clobenpropit **8** is surrounded by hydrophobic residues, L401$^{7.42}$ and W402$^{7.43}$, as shown in Fig. 5.

To understand subtype selectivity, we matched the predicted best binding pose of the highly H_3-selective ligand clobenpropit **8** at hH_3HR to other three subtypes (H_1, H_2, H_4) of hHRs, and then we used SCREAM[17] to predict the optimum side chain position of residues in the binding pocket, after which we minimized the final ligand/ protein complex post neutralization. Predicted subtype residues that vary among four subtypes (H_4: 29%, 8/28, H_1: 57%, 16/28, H_2: 68%, 19/28) are displayed in Table 4. The corresponding amino acids of conserved E5.46/ S5.43 in both of hH_3HR and hH_4HR are N198$^{5.46}$/A195$^{5.43}$ in hH_1HR and T190$^{5.46}$/ G187$^{5.43}$ (Fig. 2). Both of two subtype variable residues in hH_1HR and hH_2HR show weakened interactions in the cavity in Table 4 and Fig. 6, resulting in a 2.2 to 2.4 kcal/mol favorable interaction in hH_3HR. However, the similar interaction is shown at these two conserved residues of hH_4HR. Thus, the final cavity sum is a substantial decrease in binding affinity (cavity sum = −34.11 in hH_1HR, −33.77 in hH_2HR) in agreement with the dramatically decreased experimental binding affinity at hH_1HR (PKi: 5.6) and hH_2HR (PKi: 5.2). The final cavity sum with the weakened binding affinity at hH_4HR (PKi: 7.4) is a −35.12 kcal/mol compared with the cavity sum of hH_3HR (PKi: 9.4), −36.94 kcal/mol. Thus, this predicted binding energy is consistent with the experimental binding affinity of H_3 subtype selective clobenpropit **8**.[30] The predicted structures were ordered by experimental binding affinity including unified cavity energy (UniCav E) in Table 5 in all subtypes of hHRs. Furthermore, all scoring energies at all HRs parallel with theirs experimental binding affinities with the r^2 values (correlation coefficients) of 0.67 to 0.99 (Fig. 6A).

For further SAR studies, we included four more antagonists, ciproxifan **9**, thioperamide **10**, A-304121 **11**, and A-317920 **12** in the same literature.[30] Predicted binding cavity energies for eight models in good agreement with experimental relative binding constants (r^2=0.65 for all 8 and r^2=0.93 for 6 excluding the flexible ligands, A-304121 **11**, and A-317920 **12**, which include more than 10 rotatable bonds in their structures in Fig. 6). All of them share the same binding site with major anchoring site at D114$^{3.32}$ in Fig. 7.

Based on the docking studies of the subtype selective antagonist clobenpropit **8**, we suggest that E5.46/ S5.43 in hH_3HR and hH_4HR are involved in additional H-bonding interactions with the terminal imidazole group in the monoalkyl-substituted imidazole-based derivatives, however these interactions are lost in hH_1HR and hH_2HR, as shown in Fig. 7. Supporting this, sequence alignments show that TM5 of the hHRs is poorly conserved, suggesting a potential differences in the mechanism in which histamine binds to the hH_3HR. For the difference between hH_3HR and hH_4HR, M378$^{6.55}$ in hH_3HR (which is the corresponding amino acid of T323$^{6.55}$ in hH_4HR) stabilizes through additional hydrophobic interactions (−1.28 kcal/mol at M378$^{6.55}$ vs −0.41 kcal/mol at T323$^{6.55}$). Thus this predicted structure explains the increase of H_3 selectivity for clobenpropit **8** at hH_3HR over the other three subtypes.

In addition, scoring energy of hH_3HR selective antagonist clobenpropit for all HRs correlates with the observed experimental binding affinities with r^2 values (correlation coefficients) of 0.69 to 0.98. Docking studies were also carried out using structurally known hH_3HR selective antagonists in clinical trials, ABT-239 **1**, GSK-189,254 **2**, PF-3654746 **3**, and BF2.649 **4**. The predicted 3D models should guide the rational design of novel drugs for the subtype selective antagonists and agonists with reduced side effects. This excellent agreement with current experimental studies, particularly the understanding of subtype selectivity indicates that computationally derived structures of GPCRs can be sufficiently accurate to develop subtype selective drugs that minimizes side effects.

2.4 Docking of structurally known hH_3HR selective antagonists in clinical studies—

To develop a general pharmacophore model for these non-imidazole derivatives with hH_3HR selectivity, we selected structurally known hH_3HR targeting drugs in Phase I or II pre-clinical studies, ABT-239 **1** (pKi: 9.35), GSK-189254A **2** (pKi: 9.59), PF-3654746 **3** (pKi: 8.49), and BF2.649 **4** (tiprolisant, pKi: 8.3) for further docking studies.

As shown in Fig. 8, the binding sites of four antagonists are overlap, as expected. A central basic moiety shows common H-bonding at $D114^{3.32}$. An aromatic core structure leads to further affinity enhancing elements, e.g. hydrophilic/ lipophilic groups is surrounded by hydrophobic cavity in TMs 3-5-6 region. The aliphatic ring including a protonated nitrogen is surrounded by another hydrophobic cavity in TMs 2-3-7. GSK-189254A **2** shows an extra H-bond at $S203^{5.43}$ with the nitrogen atom in the pyridine ring. PF-3654746 **3** also forms additional H-bonding interactions among the terminal amino group, $Y194^{5.34}$, and $E206^{5.46}$, and between F substituent and $Y374^{6.51}$.

All hH_3HR selective antagonists could be mutually superposed following a common pharmacophore model with similar arrangements at the same binding site. The proposed pharmacophore model suggests the basic proton interacting with $D114^{3.32}$, the spacer, the aromatic ring substituted with the hydrophilic or lipophilic groups interacting with lipophilic pockets in TMs 3-5-6 and the aliphatic ring located in TMs 2-3-7. This model is in good agreement with the current generally accepted model; a basic amine motif separated by several atoms from the central, typically hydrophobic, core, which is joined on the other side by a structurally variable region in the form of another basic amine or a polar, non-basic arrangement (e.g. amide).[5]

3. Structure comparison of predicted structure and the experimental x-ray structure of the hH_1HR (PDB ID: 3RZE).[11]

Compared to the crystal structure of the hH_1HR, the RMSD of the predicted hH_1HR structure generated by our GEnSeMBLE method showed 1.33 Å RMSD in whole TMs, as shown in Table 6. There were also no big differences with other subtypes in the average backbone RMSD of TM helices with less than 1.64 Å for all three hH_2HR (1.64 Å), hH_3HR (1.33 Å), and hH_4HR (1.60 Å). The most similar structure of hH_1HR is hH_3HR with 0.04 Å. Among TMs major structural deviations are shown at the TMs 1 and 5 with 0.85 and 0.84 Å RMSD, respectively.

The recent availability of GPCR crystal structures provides some mechanistic insights into both the inactive and active forms, which should be useful in designing ligands for therapeutic applications. These results show that the seven-helix TM topology of these receptors can exhibit multiple conformations with variations in interhelical orientations, which in turn can change the binding site and energy of various ligands. These multiple conformations are observed both for a given GPCR in different functional forms (e.g., inactive vs. active) and across different GPCRs. The conformational variations already found in the crystallized GPCRs strongly suggest that homology models based on a single template would not be sufficiently flexible to describe the multiple functional forms of a receptor and would be unlikely to predict the important configurations of other GPCRs.

The GEnSeMBLE method applied in this paper was developed to enable exhaustive sampling of the conformational space to sample the variety of packings explored by receptors. We expect that this procedure dramatically increases the likelihood of predicting accurate structures for functionally distinct conformations of a GPCR and for predicting the structures of other more distant GPCRs. As additional GPCRs are crystallized to more fully cover both sequence space and function space (through G protein or β arrestin coupled pathways), such de novo prediction methods should increase in accuracy because of

additional templates to initiate the process. Our results indicate that starting with a template for a crystal for one subtype of a GPCR, we can obtain accurate structures for the other subtypes. Also given a crystal structure of one GPCR we can obtain accurate structures for other GPCRs that are within ~30% sequence identify for the TM regions.

CONCLUSIONS

We docking several H_3 selective ligands to all four subtypes to determine the critical components defining H_3 subtype selectivity with respect to the other three subtypes obtained by. Our predictions of the best conformations of the histamine at H_1, H_2, H_3, and H_4 receptors subtypes lead to several conclusions:

1. The largest contribution to binding of the H_3 selective agonists (**5**, **6**, **7**) is E206$^{5.46}$ in good agreement with the experimental mutational studies.
2. We find that the conserved E5.46/ S5.43 in both of hH_3HR and hH_4HR are involved in H_3/ H_4 subtype selectivity through additional H-bonding with the terminal imidazole group in the monoalkyl-substituted imidazole-based derivatives but loss of these interactions in hH_1HR and hH_2HR. In addition, M378$^{6.55}$ in hH_3HR is another subtype selective residue provides additional hydrophobic stabilization different from hH_4HR (the corresponding amino acid of T323$^{6.55}$ in hH_4HR).
3. Our proposed pharmacophore model suggests that the residues important for selectivity to hH_3HR are:
    - the basic proton interacting with D114$^{3.32}$,
    - the spacer,
    - the aromatic ring substituted with the hydrophilic or lipophilic groups interacting with lipophilic pockets in TMs 3-5-6 and
    - the aliphatic ring located in TMs 2-3-7.

We expect our predicted 3D structures for all four HRs will help guide the rational design of novel H_3 subtype selective antagonists and agonists with reduced side effects. The excellent agreement with current experimental studies, particularly the understanding of H_3 subtype selectivity indicates that computationally derived structures of GPCRs can be sufficiently accurate to develop subtype selective drug to minimize side effects.

METHODS

We used the GEnSeMBLE method[2] to predict the 3D structures for the various conformations needed to understand the function of GPCRs and help design new ligands. GEnSeMBLE provides a very complete sampling (millions to quadrillions) over possible rotations and tilts, leading to a ensemble of low lying structures expected to include those conformations energetically accessible for binding of ligands. This replaces our earlier MembStruk method.[31]

We use the DarwinDock to predict the binding sites of ligands to the GPCRs. DarwinDock samples ~ 20 conformations for ~50,000 poses expanding the predicted binding sites which we consider to be a very complete sampling. DarwinDock replaces our earlier HierDock[6] and MSCDock[32] methods, providing a much more complete sampling of possible poses. These earlier methods were validated by a series of applications to various GPCRs: human D_2 dopamine receptor (DR),[33] human β_2 adrenergic receptor,[34, 35] human M_1 muscarinic receptor,[36] human Chemokine (C-C) motif receptor 1 (CCR1),[37] mouse MrgC11 (Mas

Related Gene) for the molluscan peptide FMRF-amide (FMRFa),[38, 39] human prostanoid DP receptor,[40], human Serotonin 2C[18] and human A_{2A} adenosine[41] receptor.

1. GEnSeMBLE[41]

The structure prediction methodology has been described previously[41] so it will only be briefly summarized here:

1) **PredicTM:** Uses multiple sequence alignment to predict the TM regions for membrane protein.

2) **OptHelix/Homologize:** OptHelix generate helices with proper kinks (may be caused by Prolines) using molecular dynamics. However when closely related x-ray structures are available (as for the HRs), we find that Homology helices often provide better helix shapes.

3) **BiHelix:** This algorithm samples all N^7 packings of the 7 helices in a GPCR in which N rotations about each helix are combine. Here we consider N=13, which leads to ~63 million conformations. BiHelix partitions the 7-helix interaction problem into 12 sets of BiHelix interactions, in which SCREAM[17] is used to optimize the side-chains for each combination.

4) **CombiHelix:** The BiHelix energies for all 63,000,000 packings are used to select the best 1000. Then we build the full –helix bundle for each of these 1000 and optimize the side-chains for each using SCREAM. From this 1000 we select an ensemble of ~10 lowest energy structures each of which is used in docking of various ligands.

The Dreiding D3 force field (D3FF)[42] was used throughout wherever energies were evaluated.

2. Ligand docking

DarwinDock was used to dock several ligands to each of the lowest 10 predicted structures of all 4 hHRs from BiHelix. The starting structure and charges of the ligands in Chart 1 were calculated using density functional theory (B3LYP with the 6–311G** basis set).

Starting from the x-ray structure of histamine, we rotated the torsion angles N-C_{al}-C_{al}-C_{ar} by 60 ° increments to generate 6 conformations. These were generated with the Maestro software and minimized with the D3FF. The final docked structure with the best binding E from all ligand conformations was selected.

1) Scanning the receptor for potential binding regions—Starting with the predicted structure, we predicted putative ligands binding regions as follows. We first alanized the entire protein (replacing the 6 hydrophobic residues, I, L, V, F, Y, and W with A) and scanned for potential binding regions with no assumption about the binding site. The entire molecular surface of the predicted structure was mapped with spheres representing the empty volume of the protein (currently using the Sphgen procedure in DOCK4.0 suite of programs). The entire set of protein spheres was partitioned into ~30 to 50 overlapping cubes of 10 to 14 Å sides. We then generated 1,000 poses for each of these 30 – 50 regions. These results are compared to select the most promising two or three putative binding regions.

2) DarwinDock—For each ligand conformation, we used DarwinDock to generate iteratively ~50,000 poses spanning the putative binding regions of the bulky-residue-alanized protein. These poses are partitioned into ~1200 to ~200 family head Voronai-like

families based on RMSD. Then calculated the energies of the family heads and selected the top 10% ordered by total energy. Then we calculated the binding energy for all the family members of these top 10% family and selected the lowest energy 100 structures are chosen for further optimization. For each of these 100 we dealanize the protein side-chains (using SCREAM) to find the optimum side chains for each of the best 100 poses. Then we neutralize the protein and ligand by transferring protons appropriately within salt bridges and protonating or deprotonating exterior ligands, followed by further full geometry minimization.

DarwinDock has been validated for a number of x-ray co-crystals including 3 crystal structures of ligand/ GPCR complexes: human β_2-adrenergic receptor (0.4 Å RMSD),[15] human $AA_{2A}R$ (0.8 Å RMSD),[43] and turkey β_1-adrenergic receptor (0.1 Å RMSD).[16] This shows that DarwinDock can accurately identify ligand binding sites in proteins, which can then be used to optimize the ligands with desirable properties.

3) Neutralization for scoring E—Quantum mechanics (QM) calculations show that for an effective dielectric constant below 8, the extra proton on a Lys or Arg transfers back to the negative carboxylate of an Asp or Glu. Thus we expect that buried salt bridges will have neutral residues. We find that use of these neutral residue charges for the protein and ligand improves the accuracy for comparing different docked structures. Of course the final bond energy relative to ligand in the solvent and binding site exposed to solvent must be corrected by the effective pK_A of the ligand and of the exposed Lys, Arg, Glu, and Asp. For example, if the pK_A of a carboxylate is 4.5 and the solvent is taken to have a pH of 7.4, we must correct by 2.9*1.38 kcal/mol.

For external residues not involved in binding, we also find it is expected to neutralize the external residues exposed to solvent or membrane. Here the issue is that the force fields commonly used in molecular dynamic calculations involve fixed charges, usually based on QM. In reality any net partial charges are shielded by the dielectric polarization of the surrounding protein and solvent so that there is negligible effect beyond 10Å. However with fixed charges the electrostatic interaction energy between two point charges separated by 10Å is 33 kcal/mol. The result is that small changes in geometries of charged ligands far from the binding site can lead to large differential binding energies, even 10 to 30 kcal/mol. We find that neutralizing these exposed residues removes the sensitivity to details of the distances of charged residues (and counter ions) remote from the active site. This neutralization leads to differential binding energies that are dominated by the local cavity interactions and leads to much smaller solvation energies.[18]

Supplementary Material

Refer to Web version on PubMed Central for supplementary material.

Acknowledgments

Funding for this project was provided by gifts to the Materials and Process Simulation Center (MSC) at California Institute of Technology, Pasadena, CA. P.F. thanks the Carlsberg Foundation, Lundbeck Foundation, and the Danish Council for Independent Research | Technology and Production Sciences for financial support. In addition some funding was provided by NIH (R01NS071112 and 1R01NS073115)

REFERENCES

1. Lorenzi S, Mor M, Bordi F, Rivara S, Rivara M, Morini G, Bertoni S, Ballabeni V, Barocelli E, Plazzi PV. Validation of a histamine H3 receptor model through structure-activity relationships for classical H3 antagonists. Bioorg. Med. Chem. 2005; 13:5647–5657. [PubMed: 16085419]

2. Abrol R, Bray JK, Goddard WA III. BiHelix: Towards de novo Structure Prediction of an Ensemble of G-Protein Coupled Receptor Conformations. Proteins. 2011 DOI: 10.1002/prot.23216.
3. Nissinen MJ, Karlstedt K, Castren E, Panula P. Expression of histidine decarboxylase and cellular histamine-like immunoreactivity in rat embryogenesis. J. Histochem. Cytochem. 1995; 43:1241–1252. [PubMed: 8537641]
4. Hough LB. Genomics meets histamine receptors: New subtypes, new receptors. Mol. Pharmacol. 2001; 59:415–419. [PubMed: 11179433]
5. Berlin M, Boyce CW, de Lera Ruiz M. Histamine H3 Receptor as a Drug Discovery Target. J. Med. Chem. 2010; 54:26–53. [PubMed: 21062081]
6. Kiss R, Kiss B, Konczol A, Szalai F, Jelinek I, Laszlo V, Noszal B, Falus A, Keseru GM. Discoovery of Novel Human Histamine H4 Receptor Ligands by Large-Scale Structure-Based Virtual Screening. J. Med. Chem. 2008; 51:3145–3153. [PubMed: 18459760]
7. Carballo F. Efficiency of potent gastric acid inhibition. Drugs. 2005; 65:105–111. [PubMed: 16335864]
8. Pettit M. Treatment of gastroesophageal reflux disease. Pharm. World Sci. 2005; 27:432–435. [PubMed: 16341949]
9. Schneider EH, Strasser A, Thurmond RL, Seifert R. Structural requirements for inverse agonism and neutral antagonism of indole-, benzimidazole-, and thienopyrrole-derived histamine H4 receptor ligands. J. Pharmacol. Exp. Ther. 2010; 334:513–521. [PubMed: 20484153]
10. Ligneau X, Morisset S, Tardivel-Lacombe J, Gbahou F, Ganellin CR, Stark H, Schunack W, Schwartz J-C, Arrang J-M. Distinct Pharmacology of rat and human histamine H3 receptors: role of two amino acids in the third transmembrane domain. British J. Pharma. 2000; 131:1247–1250.
11. Shimamura T, Shiroishi M, Weyand S, Tsujimoto H, Winter G, Katritch V, Abagyan R, Cherezov V, Liu W, Han GW, Kobayashi T, Stevens RC, Iwata S. Structure of the human histamine H1 receptor complex with doxepin. Nature. 2011; 475:65–70. [PubMed: 21697825]
12. Katoh K, Kuma K, Toh H, Miyata T. MAFFT version 5: improvement in accuracy of multiple sequence alignment. Nucleic Acid Res. 2005; 33:511–518. [PubMed: 15661851]
13. Wimley WC, Creamer TP, White SH. Solvation energies of amino acid side chains and backbone in a family of host-guest pentapeptides. Biochem. 1996; 35:5109–5124. [PubMed: 8611495]
14. Hessa TM-B, Bernsel A, Kim H, Sato Y, Lerch-Bader M, Nilsson I, White SH, von Heijne G. Molecular code for transmembrane-helix recognition by the Sec61 translocon. Nature. 2007; 450:1026–1030. [PubMed: 18075582]
15. Cherezov V, Rosenbaum DM, Hanson MA, Rasmussen SGF, Thian FS, Kobilka TS, Choi H-J, Kuhn P, Weis WI, Kobilka BK, Stevens RC. High-resolution crystal structure of an engineered human beta2-adrenergic G protein-coupled receptor. Sci. 2007; 318:1258–1265.
16. Warne T, Serrano-Vega MJ, Baker JG, Moukhametzianov R, Edwards PC, Henderson R, Leslie AGW, Tate CG, Schertler GFX. Structure of a β1-adrenergic G-protein coupled receptor. Nature. 2008; 454:486–491. [PubMed: 18594507]
17. Kam VWT, Goddard WA III. Flat-Bottom Strategy for Improved Accuracy in Protein Side-Chain Placements. J. Chem. Theo. & Comp. 2008; 4:2160–2169.
18. Bray JK, Goddard WA III. The structure of human serotonin 2c G-protein-coupled receptor bound to agonists and antagonists. J. Mol. Graph. Model. 2008; 27:66–81. [PubMed: 18499489]
19. Venable JD, Thurmond RL. Development and chemistry of histamine H4 receptor ligands as potential modulators of inflamationary and allergic diseases. Anti-Inflamm. Anti-Allergy Agents in Med. Chem. 2006; 5:307–322.
20. Stark H, Kathmann M, Schlicker E, Schunack W, Schlegel B, Sippl W. Medicinal chemical and pharmacological aspects of imidazole-containing histamine H3 receptor antagonists. Mini Rev. Med. Chem. 2004; 4:965–977. [PubMed: 15544557]
21. Letavic MA. Recent medicinal chemistry of the histmine H3 receptor. Prog. Med. Chem. 2006; 44:181–206. [PubMed: 16697898]
22. Brioni JD, Esbenshade TA, Garrison TR, Bitner SR, Cowart MD. Discovery of Histamine H3 Antagonists for the Treatment of Cognitive Discorders and Alzheimer's Disease. J. Pharmacol. Exp. Ther. 2011; 336:38–46. [PubMed: 20864505]

23. Esbenshade TA, Fox GBK,KM, Miller TR, Kang CH, Denny LI, Witte DG, Yao BB, Pan L, Wetter J, Marsh K, Bennani YL, Cowart MD, Sullivan JP, Hancock AA. Pharmacological properties of ABT-239 [4-(2-{2-[(2R)-2-Methylpyrrolidinyl]ethyl}-benzofuran-5-yl)benzonitrile]: I. Potent and selective histamine H3 receptor antagonist with drug-like properties. J. Pharmacol. Exp. Ther. 2005; 313:165–175. [PubMed: 15608078]
24. Medhurst AD, Atkins AR, Beresford IJ, Brackenborough K, Briggs MA, Calver AR, Cilia J, Cluderay JE, Crook B, Davis JB, Davis RK, Davis RP, Dawson LA, Foley AG, Gartlon J, Gonzalez MI, Heslop T, Hirst WD, Jennings C, Jones DN, Lacroix LP, Martyn A, Ociepka S, Ray A, Regan CM, Roberts JC, Schogger J, Southam E, Stean TO, Trail BK, Upton N, Wadsworth G, Wald JA, White T, Witherington J, Woolley ML, Worby A, Wilson DM. GSK189254, a novel H3 receptor antagonist that binds to histamine H3 receptors in Alzheimer's disease brain and improves cognitive performance in preclinical models. J. Pharmacol. Exp. Ther. 2007; 321:1032–1045. [PubMed: 17327487]
25. Ligneau X, Perrin D, Landais L, Camelin JC, Calmels TP, I. B-B, Lecomte JM, Parmentier R, Anaclet C, Lin JS, Bertaina-Anglade V, la Rochelle CD, d'Aniello F, Rouleau A, Gbahou F, Arrang JM, Ganellin CR, Stark H, Schunack W, Schwartz JC. BF2.649 [1-{3-[3-(4-Chlorophenyl)propoxy]propyl}piperidine, Hydrochloride], a Nonimidazole Inverse Agonist/Antagonist at the Human Histamine H3 Receptor: Preclinical Pharmacology. J. Pharmacol. Exp. Ther. 2007; 320:365–375. [PubMed: 17005916]
26. Uveges AJ, Kowal D, Zhang Y, Spangler TB, Dunlop J, Semus S, Jones PG. The role of transmembnane Helix 5 in agonist binding to the human H3 receptor. J. Pharmacol. Exp. Ther. 2002; 301:451–458. [PubMed: 11961043]
27. Shin N, Coates E, Murgolo NJ, Morse KL, Bayne M, Strader CD, Monsma FJ Jr. Moledular modeling and site-specific mutagenesis of the histamine-binding site of the histamine H4 receptor. Mol. Pharmacol. 2002; 62:38–47. [PubMed: 12065753]
28. Jongejan A, Lim HD, Smits RA, de Esch IJP, Haaksma E, Leurs R. Delineation of agonist binding to the human histamine H4 receptor using mutational analysis, homology modeling, and ab initio calculations. J. Chem. Inf. Model. 2008; 48:1455–1463. [PubMed: 18553960]
29. Lim HD, van Rijn RM, Ling P, Bakker RA, Thurmond RL, Leurs R. Evaluation of Histamine H1-,H2-, and H3-Receptor Ligands at the Human Histamine H4 Receptor: Identification of 4-Methylhistamine as the First Potent and Selective H4 Receptor Agonist. J. Pharmacol. Exp. Ther. 2005; 314:1310–1321. [PubMed: 15947036]
30. Esbenshade TA, Krueger KM, Miller TR, Kang CH, Denny LI, Witte DG, Yao BB, Fox GB, Faghih R, Bennani YL, Williams M, Hancock AA. Two novel and selective nonimidazole histamine H3 receptor antagonists A-304121 and A-317920: I. In vitro pharmacological effects. J. Pharmacol. Exp. Ther. 2003; 305:887–896. [PubMed: 12606603]
31. Vaidehi N, Floriano WB, Trabanino R, Hall SE, Freddolino P, Choi EJ, Goddard WA III. Structure and Function of GPCRs. Proc. Natl. Acad. Sci. USA. 2002; 99:12622–12627. [PubMed: 12351677]
32. Cho AE, Wendel JA, Vaidehi N, Kekenes-Huskey PM, Floriano WB, Maiti PK, Goddard WA III. The MPSim-Dock Hierarchical Docking Algorithm: Application to the eight trypsin Inhibitor co-crystals. J. Comp. Chem. 2005; 26:48–71. [PubMed: 15529328]
33. Kalani Y, Vaidehi N, Hall SE, Floriano WB, Trabanino RJ, Freddolino PL, Kam V, Goddard WA III. Three-dimensional structure of the human D2 dopamine receptor and the binding site and binding affinities for agonists and antagonists. Proc. Natl. Acad. Sci. USA. 2004; 101:3815–3820. [PubMed: 14999101]
34. Freddolino PL, Kalani MY, Vaidehi N, Floriano WB, Trabanino RJ, Freddolino PL, Kam V, Goddard WA III. Structure and function prediction for human b2- adrenergic receptor. Proc. Natl. Acad. Sci. USA. 2004; 101:2736–2741. [PubMed: 14981238]
35. Spijker P, Vaidehi N, Freddolino PL, Hilbers PA, Goddard WA III. Dynamic behavior of fully solvated b2-adrenergic receptor, embedded in the membrane with bound agonist or antagonist. Proc. Natl. Acad. Sci., USA. 2006; 103:4882–4887. [PubMed: 16551744]
36. Peng JY, Vaidehi N, Hall SE, Goddard WA III. The Predicted 3D Structures of the Human M1 Muscarinic Acetylcholine Receptor with Agonist or Antagonist Bound. Chem. Med. Chem. 2006; 1:878–890. [PubMed: 16902941]

37. Vaidehi N, Schlyer S, Trabanino RJ, Floriano WB, R. A, Sharma S, Kochanny M, Koovakat S, Dunning L, Liang M, Fox JM, de Mendonca FL, Pease JE, Goddard WA III, Horuk R. Predictions of CCR1 Chemokine Receptor Structure and BX 471 Antagonist Binding Followed by Experimental Validation. J. Biol. Chem. 2006; 281:27613–27620. [PubMed: 16837468]

38. Heo J, Han S-K, Vaidehi N, Wendel J, Kekenes-Huskey P, Goddard WA III. Prediction of the 3D Structure of FMRF-amide Neutopeptides Bound to the Mouse MrgC11 GPCR and Experimental Validation. Chem. Bio. Chem. 2007; 8:1527–1539.

39. Heo J, Vaidehi N, Wendel J, Goddard WA III. Prediction of the 3-D structure of rat MrgA G protein-coupled receptor and identification of its binding site. J. Mol. Graph. Model. 2007; 26:800–812. [PubMed: 17728165]

40. Li Y, Zhu F, Vaidehi N, Goddard WA III, Sheinerman F, Reiling S, Morize I, Mu L, Harris K, Ardati A, Laoui A. Prediction of the 3D structure and dynamics of human DP G-protein coupled receptor bound to an agonist and an antagonist. J. Am. Chem. Soc. 2007; 129:10720–10731. [PubMed: 17691773]

41. Goddard WA III, Kim S-K, Li Y, Trzaskowski B, Griffith AR, Abrol R. Predicted 3D structures for adenosine receptors bound to ligands: Comparison to the crystal structure. J. Struct. Biol. 2010; 170:10–20. [PubMed: 20079848]

42. Mayo SL, Olafson BD, Goddard WA III. DREIDING - a generic force field for molecular simulations. J. Phys. Chem. 1990; 94:8897–8909.

43. Jaakola VP, Griffith MT, Hanson MA, Cherezov V, Chien EY, Lane JR, Ijzerman AP, Stevens RC. The 2.6 angstrom crystal structure of a human A2A adenosine receptor bound to an antagonist. Sci. 2008; 322:1211–1277.

BRIEFS

We report here the predicted structure of the human H_3 Histamine receptor bound to highly potent and selective H_3 selective agonists and antagonists.

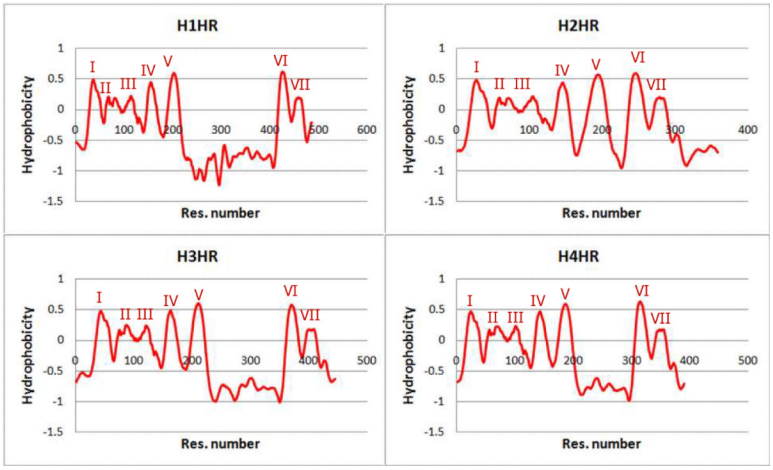

Figure 1.
The hydropathy prediction from PredicTM for the four histamine receptors (HR).

Figure 2.

Alignments of the four histamine (HR) subtypes, H_1, H_2, H_3, and H_4 from the PredicTM method. The predicted transmembrane (TM) regions from PredicTM are displayed in colored boxes (TM1 in purple, TM2 in blue, TM3 in cyan, TM4 in green, TM5 in yellow, TM6 in orange, TM7 in red). Highly conserved residues in Family A G protein-coupled receptors (GPCRs) are shown in red in TM 1–6 and white in TM7. Variable amino acids among the four subtypes in the upper TM regions are marked with red asterisks and subtype selective residues predicted from the cavity analysis are boxed. We use Ballesteros-Weinstein numbering consisting of the TM helix number followed by residue number relative to the highly conserved residue in the helix, numbered as 50. H-bonding is indicated by arrows, and subtype selective residues are shown in red.

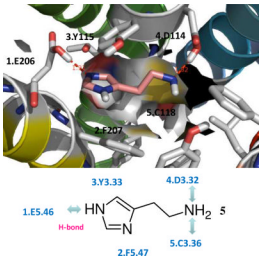

Figure 3.

Predicted best models of the endogenous agonist histamine **5** bound to the human histamine H_3 receptor (hH_3HR). The H-bonding is represented by the arrows with the distance between the donor and the acceptor. The number with residue is from the order of unified cavity E in Table 2. Schematic structure of the predicted binding sites is displayed in the bottom figure.

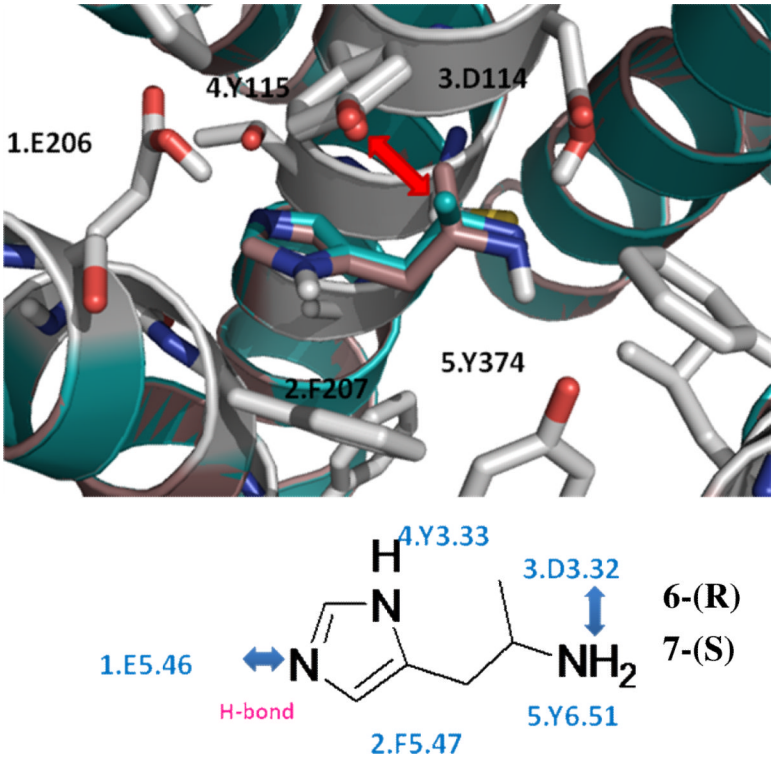

Figure 4.

Superposition of the H_3 selective agonist (*R*)-α-methyl histamine **6** and (*S*)-α-methyl histamine **7** to the human histamine H_3 receptor (hH_3HR). The H-bonding is represented by the arrows between the donor and the acceptor. (*S*)-α-methyl histamine with ~ 100-fold less binding affinity displayed unfavorable interaction at Y115 with α-methyl groups in red arrow. The number with residue is from the order of unified cavity E in Table 3. Schematic structure of the predicted binding sites is displayed in the bottom figure.

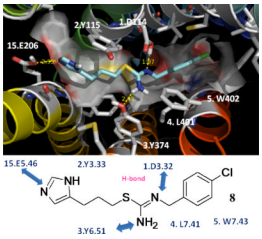

Figure 5.

Predicted best models of the H_3 selective antagonist clobenpropit **8** bound to the human histamine H_3 receptor (hH_3HR). The H-bonding is represented by the arrows between the donor and the acceptor. The number with residue is from the order of unified cavity E in Table 5. Schematic structure of the predicted binding sites is displayed in the bottom figure.

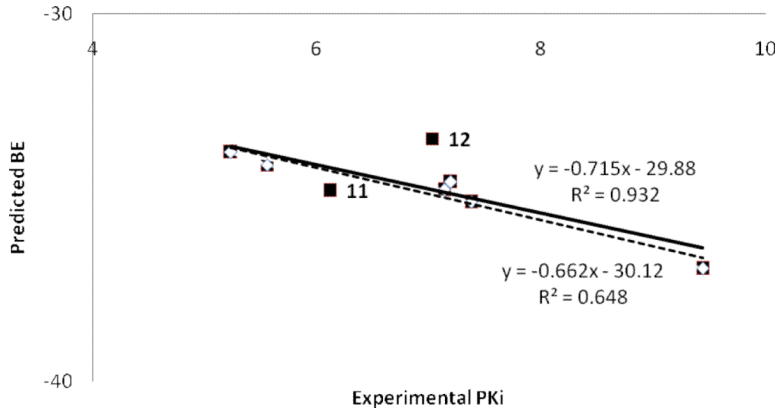

Figure 6.

The predicted binding energies (kcal/mol) to the H_3 selective antagonist clobenpropit **8** bound to four human histamine receptors (hH_1HR, hH_2HR, hH_3HR, hH_4HR) and other antagonists, ciproxifan **9**, thioperamide **10**, A-304121 **11**, and A-317920 **12** at hH_3HR listed in Table 5 compared with the experimental binding constants (pK_i). The dotted line shows the fit without two outliers, **11** and **12**, (which is much more flexible than the others).

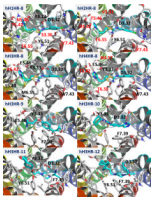

Figure 7.

Predicted best models of the H_3 selective antagonist clobenpropit **8** bound to four human histamine receptors (hH_1HR, hH_2HR, hH_3HR, hH_4HR) and other antagonists, ciproxifan **9**, thioperamide **10**, A-304121 **11**, and A-317920 **12** at hH_3HR. H-bonding is indicated by red dots, and subtype selective residues are shown in red.

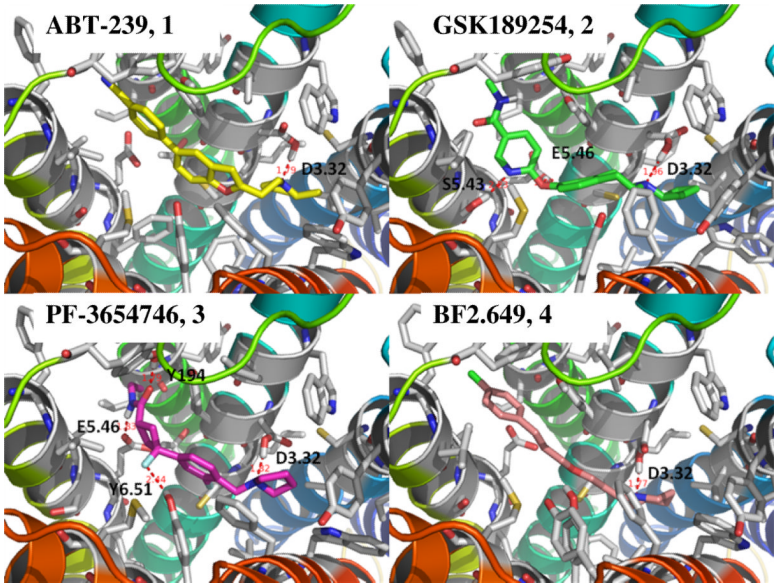

Figure 8.

Predicted binding sites of structurally known human histamine H_3 receptor (hH_3HR) in clinical study, ABT-239 **1**, GSK-189,254 **2**, and PF-3654746 **3**, and BF2.649 (Tiprolisant) **4** at hHH_3R. H-bonding is indicated by red dots.

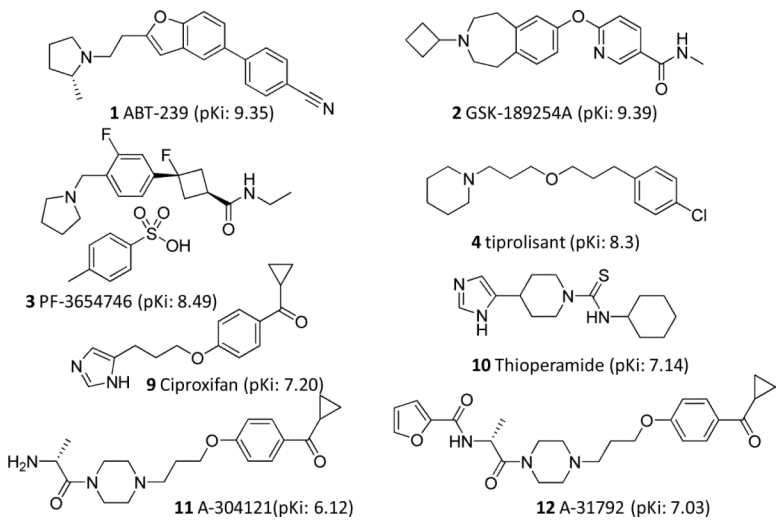

Chart 1.

The chemical structures of structurally known histamine H_3 receptor antagonists in clinical study, ABT-239 **1**, GSK-189254A **2**, PF-3654746 **3**, and BF2.649 (Tiprolisant) **4**. Binding affinities (pK_i) are shown for H_3 with its function in parenthesis compared to the endogenous histamine.

Table 1

Top 10 predicted structures of the four human histamine receptors (hHRs) from the CombiHelix analysis of the $(13)^7$ = 62,748,517 BiHelix packing geometries within ± 90 ° angle range by 15 ° increments. All 1,000 models from CombiHelix were selected for neutralization by their charge total energy (E) score (ChargeTot: kcal/mol). The final 100 models were ordered by neutral total E (NeutTot: kcal/mol). The case with η = 0 ° for all 7 helices is represented in *italic* and the best E is shown in grey shading.

hH_1HR-β2Hom

#	H1	H2	H3	H4	H5	H6	H7	CIH	CTot	NIH	NTot
H1-1	0	0	0	15	0	0	0	**−229.2**	**803.0**	−387.6	**354.2**
H1-2	*0*	*0*	*0*	*0*	*0*	*0*	*0*	*−207.4*	*816.7*	*−374.6*	*358.0*
H1-3	0	0	0	−15	0	0	0	−245.1	814.0	**−388.8**	376.4
H1-4	0	0	0	0	0	0	90	−171.0	861.0	−360.8	387.9
H1-5	0	0	0	0	0	−15	0	−168.6	852.6	−344.5	395.1
H1-6	0	−15	0	0	0	0	0	−204.8	847.9	−365.0	395.9
H1-7	−15	0	0	15	0	0	0	−217.5	852.7	−380.5	395.9
H1-8	90	0	0	0	0	0	0	−183.4	849.1	−341.9	399.1
H1-9	−15	0	0	0	0	0	0	−190.2	840.2	−358.7	401.3
H1-10	0	0	0	30	0	0	0	−200.6	846.5	−365.3	401.8

hH_2HR-β1Hom

#	H1	H2	H3	H4	H5	H6	H7	CIH	CTot	NIH	NTot
H2-1	0	0	0	−15	0	0	0	**−502.8**	**51.0**	**−390.7**	**33.9**
H2-2	−75	0	0	−15	0	0	90	−462.7	78.9	−354.6	56.0
H2-3	0	0	0	−15	0	0	90	−466.6	106.7	−372.9	64.6
H2-4	−90	0	0	−15	0	0	−15	−478.8	77.6	−361.0	65.8
H2-5	−90	0	0	−15	0	0	90	−446.5	99.7	−348.0	66.8
H2-6	*0*	*0*	*0*	*0*	*0*	*0*	*0*	*−487.9*	*98.6*	*−380.4*	*67.2*
H2-7	−90	0	0	−15	0	45	−30	−470.4	94.4	−351.1	71.0
H2-8	−15	0	0	−15	0	0	0	−482.4	92.9	−366.4	78.0
H2-9	0	0	0	−15	−15	0	0	−479.4	91.1	−374.5	78.7
H2-10	−15	0	0	−15	0	0	90	−441.1	130.8	−345.5	85.9

hH$_3$HR-β2*

#	H1	H2	H3	H4	H5	H6	H7	CIH	CTot	NIH	NTot
H3-1	0	0	0	−30	0	0	0	−423.8	413.8	−372.1	**16.6**
H3-2	0	0	15	−15	15	0	0	−385.1	437.2	**−374.2**	18.8
H3-3	0	0	0	−15	0	0	0	**−426.5**	429.9	−376.7	22.4
H3-4	0	0	15	−30	15	0	0	−380.9	422.9	−337.4	31.0
H3-5	0	0	0	30	0	0	0	−393.6	425.4	−364.4	34.3
H3-6	0	0	15	30	0	0	0	−338.3	439.8	−328.6	35.5
H3-7	0	0	−15	30	0	0	0	−347.2	**411.8**	−337.5	35.9
H3-8	0	0	15	−30	0	0	0	−390.7	435.3	−346.4	38.7
H3-9	0	0	15	45	15	0	0	−325.3	444.0	−323.2	40.0
H3-10	0	0	15	−30	0	15	0	−392.0	437.0	−357.6	40.6

hH$_4$HR-β1*

#	H1	H2	H3	H4	H5	H6	H7	CIH	CTot	NIH	NTot
H4-1	0	0	0	0	15	0	0	−503.7	**406.1**	−399.7	**226.0**
H4-2	0	0	0	−15	15	0	0	−510.5	409.1	−394.8	244.5
H4-3	0	0	0	15	15	0	0	−494.1	433.3	−392.6	245.1
H4-4	0	0	0	15	15	45	−15	−475.6	441.7	−357.8	257.4
H4-5	0	0	0	0	15	0	15	−497.1	443.9	−392.2	259.1
H4-6	0	0	0	0	15	45	−15	−486.1	425.1	−376.3	259.2
H4-7	0	0	0	15	15	0	−15	−491.9	450.9	**−401.5**	260.7
H4-8	0	0	0	−15	0	0	0	−522.2	432.9	−378.0	261.8
H4-9	0	0	0	−15	15	0	15	**−523.8**	431.3	−400.2	263.0
H4-10	0	0	0	0	15	0	−15	−460.8	477.6	−380.6	270.9

- CIH (Charge interhelical energy), CTot (Charge total energy), NIH (Neutral interhelical energy), NTot (Neutral total energy)

* The case with η = 0 ° for all 7 helices is ranked as 12 (E: 43.6 kcal/ mol) in hH3HR-β 2 and 34 in hH4HR-β 1 (E: 298.9 kcal/ mol), respectively.

Table 2

Cavity energy of the endogenous agonist histamine bound to the human histamine H_3 receptor (hH_3HR).

Res. #	vdW	Coulomb	H-Bond	NonBond	Mutation	Ki (nM)
E206	1.69	−2.80	−3.97	−5.08	**E206A**	32550.00
F207	−4.00	0.18	0.00	−3.81		
Y115	−2.91	−0.17	0.00	−3.09		
D114	4.42	−1.89	−4.66	−2.12		
C118	1.00	−0.17	−1.47	−0.64		
Y374	−0.48	−0.12	0.00	−0.60		
T119	−0.66	0.17	0.00	−0.49		
Y167	−0.45	−0.03	0.00	−0.47		
L401	−0.48	0.05	0.00	−0.43		
F398	−0.28	−0.06	0.00	−0.33		
T204	−0.29	0.00	0.00	−0.30	**T204A**	91.00
W371	−0.22	−0.06	0.00	−0.28		
M378	−0.25	−0.03	0.00	−0.28		
S203	−0.31	0.13	0.00	−0.18		
F211	−0.15	−0.01	0.00	−0.16		
L111	−0.13	0.03	0.00	−0.10		
W174	−0.07	−0.01	0.00	−0.08		
I171	−0.04	−0.03	0.00	−0.07		
W402	−0.02	0.00	0.00	−0.02		
A202	−0.09	0.10	0.00	0.01	**A202Q**	66.68
SUM				**−18.52**	**WT**	15.86

- Residues are ordered by total NonBond energy, which is the sum of van der Waals (vdW), Coulomb, and H-bond energy (kcal/mol) in the unified cavity.

- The color coding for contributions of each residue to binding of the adenosine ligand is: Dark grey: > 3 kcal/mol, Grey: 1 – 3 kcal/mol, Light grey: 0.5 – 1.0 kcal/mol.

- The experimental point-mutation result was compared.

Table 3

Cavity energy of the H3 selective agonist (*R*)-α-methyl histamine vs (*S*)-α-methyl histamine at the human H_3 histamine receptor (hH_3HR).

Res. #	(*R*)-α-methyl histamine (Pki: 8.2)				(*S*)-α-methyl histamine (Pki: 7.2)			
	VdW	**Coulomb**	**H-Bond**	**NonBond**	**VdW**	**Coulomb**	**H-Bond**	**NonBond**
E206	2.50	−2.91	−4.31	−4.73	1.41	−2.82	−4.00	−5.41
F207	−4.15	0.16	0.00	−3.99	−3.54	0.06	0.00	−3.49
D114	3.48	−1.89	−4.55	−2.96	2.17	−1.19	−3.67	−2.69
Y115	*−2.13*	*−0.25*	*0.00*	*−2.38*	*6.97*	*−0.13*	*0.00*	*6.84*
Y374	−0.66	−0.15	0.00	−0.81	−0.69	−0.16	0.00	−0.85
T119	−0.70	0.15	0.00	−0.56	−0.66	0.19	0.00	−0.47
Y167	−0.50	−0.02	0.00	−0.52	−0.49	−0.04	0.00	−0.53
F398	−0.48	−0.04	0.00	−0.52	−0.38	−0.06	0.00	−0.44
L401	−0.48	0.05	0.00	−0.43	−0.13	0.05	0.00	−0.08
M378	−0.29	−0.03	0.00	−0.32	−0.30	−0.03	0.00	−0.32
W371	−0.26	−0.06	0.00	−0.31	−0.29	−0.06	0.00	−0.35
T204	−0.30	0.01	0.00	−0.30	−0.31	0.02	0.00	−0.29
S203	−0.45	0.18	0.00	−0.28	−0.57	0.28	0.00	−0.29
F211	−0.17	−0.02	0.00	−0.18	−0.18	−0.02	0.00	−0.20
L111	−0.20	0.05	0.00	−0.15	−0.20	0.00	0.00	−0.20
L117	−0.16	0.05	0.00	−0.12	−0.20	0.06	0.00	−0.14
W174	−0.09	0.00	0.00	−0.10	−0.08	0.00	0.00	−0.09
I171	−0.05	−0.03	0.00	−0.08	−0.05	−0.03	0.00	−0.07
V83	−0.09	0.01	0.00	−0.08	−0.10	0.01	0.00	−0.09
C118	3.53	−0.22	−2.58	0.73	2.28	−0.14	−1.41	0.73
SUM				**−18.07**				**− 8.39**

- Residues are ordered by total NonBond energy of (*R*)-methyl histamine, which is the sum of van der Waals (vdW), Coulomb, and H-bond energy (kcal/mol) in the unified cavity.

- (*S*)-α-methyl histamine with ~ 100-fold less binding affinity[29] displayed unfavorable interaction at Y115 with α-methyl groups in *italic* font.

- The color coding for contributions of each residue to binding of the adenosine ligand is: Dark grey: > 3 kcal/mol, Grey: 1 – 3 kcal/mol, Light grey: 0.5 – 1.0 kcal/mol.

Table 4

Cavity energy of the H_3 selective antagonist clobenpropit **8** to four human histamine receptors (HRs).

Ballesteros-Weinstein #	hH_3HR (pKi: 9.4)		hH_4HR (pKi: 7.4)		hH_1HR (pKi: 5.6)		hH_2HR (pKi: 5.2)	
	Res. #	NonBond	Res. #	NonBond	Res. #	NonBond	Res. #	NonBond
3.33	Y115	−4.96	Y95	−5.70	Y108	−5.41	*V99*	*−3.45*
7.43	W402	−4.71	W348	−5.20	*Y458*	*−4.02*	*Y278*	*−2.78*
3.32	D114	−3.73	D94	−3.55	D107	−2.73	D98	−5.19
6.51	Y374	−2.54	Y319	−2.51	Y431	−3.65	Y250	−3.19
5.43	S203	−2.43	S179	−1.79	*A195*	*−0.53*	*G187*	*−1.21*
5.46	E206	−2.22	E182	−3.39	*N198*	*−1.92*	*T190*	*−1.07*
3.28	W110	−1.68	W90	0.00	W103	−1.60	*Y94*	*0.00*
3.36	C118	−1.66	C98	−3.11	*S111*	*−3.63*	C102	−2.80
2.57	C87	−1.58	*S68*	*−2.02*	*V80*	*−1.47*	*V71*	*−2.24*
2.53	V83	−1.33	V64	−1.26	V76	2.25	*L67*	*0.15*
6.55	M378	−1.28	*T323*	*−0.41*	*F435*	*−1.66*	*F254*	*−2.40*
2.51	Y81	−1.27	Y72	−1.35	*N84*	*−0.84*	*S75*	*−0.67*
7.39	F398	−1.20	F344	−0.12	*I454*	*−1.12*	*L274*	*−0.98*
6.48	W371	−1.14	W316	−0.58	W428	−1.51	W247	−2.83
2.58	I88	−1.03	I69	−0.78	*M81*	*0.14*	*L72*	*−1.25*
5.47	F207	−0.77	F183	−1.07	F199	−0.48	F191	−0.83
3.35	L117	−0.75	L97	−0.95	*A110*	*−0.65*	L101	−0.73
3.37	T119	−0.74	T99	−0.50	T112	−0.74	T103	−0.39
6.52	T375	−0.60	*S320*	*−0.24*	*F432*	*−1.06*	*F251*	*−0.81*
5.39	L199	−0.57	L175	−0.45	*K191*	*−0.22*	*G183*	*−0.22*
5.42	L401	−0.39	*Q347*	*0.03*	*G457*	*−0.22*	*G457*	*0.00*
3.31	V113	−0.34	*T93*	*−0.43*	*M106*	*−0.41*	*L97*	*0.00*
5.38	F198	−0.15	*I174*	*−0.14*	F190	0.00	*Y182*	*0.00*
4.57	Y167	0.00	*N147*	*0.15*	V159	−0.64	*S150*	*0.00*
4.61	I171	0.00	I151	0.00	*L163*	*−0.31*	I154	0.00
7.40	W399	0.00	W345	0.00	W455	0.00	W275	−0.75

Ballesteros-Weinstein #	hH_3HR (pKi: 9.4)		hH_4HR (pKi: 7.4)		hH_1HR (pKi: 5.6)		hH_2HR (pKi: 5.2)	
	Res. #	**NonBond**	**Res. #**	**NonBond**	**Res. #**	**NonBond**	**Res. #**	**NonBond**
7.46	S405	0.00	S351	0.00	S461	−0.23	S281	0.00
5.42	A202	0.13	*T178*	*0.23*	*T194*	*−1.47*	*D186*	*−0.13*
	SUM	**−36.94**	**SUM**	**−35.12**	**SUM**	**−34.11**	**SUM**	**−33.77**

- Residues are ordered by total NonBond energy (H3), which is the sum of van der Waals (vdW), Coulomb, and H-bond energy (kcal/mol) in the unified cavity.

- Predicted subtype residues that vary among four subtypes (H4: 29%, 8/28, H1: 57%, 16/28, H2: 68%, 19/28) are displayed in *italic* font.

- The color coding for contributions of each residue to binding of the adenosine ligand is: Dark grey: > 3 kcal/mol, Grey: 1 – 3 kcal/mol, Light grey: 0.5 – 1.0 kcal/mol.

- In the Ballesteros-Weinstein numbering, the most conserved residue in each of the 7 TM domains is taken as the reference and numbered as 50. This residue is designated x.50 where x is the number of the TM helix.

Table 5

Calculated binding energies (E, kcals/mols) of the H_3 selective antagonist clobenpropit 8 bound to four human histamine receptors (HR) and other antagonists (ciproxifan **9**, thioperamide **10**, A-304121 **11**, A-317920 **12** at hH_3HR. Energetically favorable E is in grey shading.

Compound/ hHRs	pKi	LocalCav	UnifiedCav	Snapbe	SnapbeSolv
Clobenpropit/ hH_3HR	9.44	−36.94	−38.29	−61.09	−48.85
Clobenpropit/ hH_4HR	7.38	−35.12	−36.07	−56.62	−45.06
Ciproxifan/ hH_3HR	7.20	−34.58	−35.85	−42.48	−30.18
Thioperamide/ hH_3HR	7.14	−34.79	−36.93	−45.33	−32.32
A-317920/ hH_3HR	7.03	−33.40	−36.88	−59.12	−41.60
A-304121/ hH_3HR	6.12	−34.81	−37.41	−69.14	−53.57
Clobenpropit/ hH_1HR	5.56	−34.11	−35.01	−55.29	−44.33
Clobenpropit/ hH_2HR	5.24	−33.77	−34.30	−48.46	−36.20

- LocalCav: Local cavity E, UnifiedCav: Unified cavity E, Snapbe: Snap binding E = Complex E − (Protein E − Ligand E), SnapbeSol: Snap binding E including solvation E with Delphi method

Table 6

RMSD matrix between predicted histamine receptors (top1 from BiHelix in Table 1) and the recently reported 3.1 Å crystal structure of the hH_1HR (PDB ID: 3RZE).[11]

All TMs	hH1HR	hH2HR	hH3HR	hH4HR	3RZE
hH1HR	0.00	1.03	0.04	1.01	1.33
hH2HR	1.03	0.00	1.03	0.23	1.64
hH3HR	0.04	1.03	0.00	1.01	1.33
hH4HR	1.01	0.23	1.01	0.00	1.60
3RZE	1.33	1.64	1.33	1.60	0.00

TM1	hH1HR	hH2HR	hH3HR	hH4HR	3RZE
hH1HR	0.00	0.41	0.05	0.35	0.85
hH2HR	0.41	0.400	0.410	0.19	1.00
hH3HR	0.05	**0.0**	0.00	0.33	0.84
hH4HR	0.35	0.19	0.33	0.00	0.92
3RZE	0.85	1.00	0.84	0.92	0.00

TM2	hH1HR	hH2HR	hH3HR	hH4HR	3RZE
hH1HR	0.00	0.41	0.05	0.45	0.65
hH2HR	0.41	0.00	0.41	0.24	0.68
hH3HR	0.05	0.41	0.00	0.44	0.66
hH4HR	0.45	0.24	0.44	0.00	0.72
3RZE	0.65	0.68	0.66	0.72	0.00

TM3	hH1HR	hH2HR	hH3HR	hH4HR	3RZE
hH1HR	0.00	0.26	0.04	0.27	0.57
hH2HR	0.26	0.00	0.26	0.17	0.68
hH3HR	0.04	0.26	0.00	0.27	0.57
hH4HR	0.27	0.17	0.27	0.00	0.67
3RZE	0.57	0.68	0.57	0.67	0.00

TM4	hH1HR	hH2HR	hH3HR	hH4HR	3RZE
hH1HR	0.00	0.47	0.04	0.40	0.84
hH2HR	0.47	0.00	0.48	0.23	0.97
hH3HR	0.04	0.48	0.00	0.41	0.85
hH4HR	0.40	0.23	0.41	0.00	0.93
3RZE	0.84	0.97	0.85	0.93	0.00

TM5	hH1HR	hH2HR	hH3HR	hH4HR	3RZE
hH1HR	0.00	0.21	0.03	0.22	0.67
hH2HR	0.21	0.00	0.21	0.18	0.61
hH3HR	0.03	0.21	0.00	0.22	0.66
hH4HR	0.22	0.18	0.22	0.00	0.58
3RZE	0.67	0.61	0.66	0.58	0.00

TM6	hH1HR	hH2HR	hH3HR	hH4HR	3RZE
hH1HR	0.00	0.34	0.03	0.36	0.73
hH2HR	0.34	0.00	0.33	0.16	0.73
hH3HR	0.03	0.33	0.00	0.36	0.73
hH4HR	0.36	0.16	0.36	0.00	0.70
3RZE	0.73	0.73	0.73	0.73	0.00

TM7	hH1HR	hH2HR	hH3HR	hH4HR	3RZE
hH1HR	0.00	0.32	0.03	0.34	0.79
hH2HR	0.32	0.00	0.32	0.27	0.71
hH3HR	0.03	0.32	0.00	0.35	0.79
hH4HR	0.34	0.27	0.35	0.00	0.69
3RZE	0.79	0.71	0.79	0.69	0.00